144
2-10-81
gwb

R 1876

(2)

Dr. 2282

ORNL/TM-7571

ornl

OAK RIDGE NATIONAL LABORATORY

UNION CARBIDE

Characterization of SiC Coatings on HTGR Fuel Particles: Final Report

R. J. Lauf
D. N. Braski

MASTER

METALS and CERAMICS
ENERGY
RESEARCH
DEVELOPMENT
OAK RIDGE NATIONAL LABORATORY

OPERATED BY
UNION CARBIDE CORPORATION
FOR THE UNITED STATES
DEPARTMENT OF ENERGY

ORNL/TM-7571
Distribution
Category UC-77

Contract No. W-7405-eng-26

METALS AND CERAMICS DIVISION

HTGR BASE TECHNOLOGY PROGRAM

Fueled Graphite Development (FTP/A 01330)

CHARACTERIZATION OF SiC COATINGS ON HTGR FUEL PARTICLES: FINAL REPORT

R. J. Lauf and D. N. Braski

Date Published: January 1981

OAK RIDGE NATIONAL LABORATORY
Oak Ridge, Tennessee 37830
operated by
UNION CARBIDE CORPORATION
for the
DEPARTMENT OF ENERGY

CONTENTS

CHARACTERIZATION OF SiC COATINGS ON HTGR FUEL PARTICLES: FINAL REPORT

R. J. Lauf and D. N. Braski

ABSTRACT

Fuel particles for the HTGR contain a layer of pyrolytic silicon carbide to act as a pressure vessel and fission product barrier. The SiC is deposited by thermal decomposition of methyltrichlorosilane (CH_3SiCl_3 or MTS) in an excess of hydrogen. Coatings deposited at temperatures from 1500 to 1700°C and coating rates from 0.4 to 1.2 μm/min have been studied by transmission electron microscopy, small-angle x-ray scattering, x-ray diffraction, optical microscopy, density measurements, scanning electron microscopy, and microhardness measurements. Transmission electron microscopy has the necessary resolution to provide crystallographic information on small coating defects. Major defects were voids, stacking faults, and dislocations. Small-angle x-ray scattering was used to measure the void size distribution; voids were generally from 20 to 80 nm in diameter. X-ray diffraction indicates that SiC coatings are predominantly cubic β-SiC. However, the high stacking fault density in some coatings can give rise to both x-ray and electron diffraction effects. In some small areas the faulted structure resembles one or more polytypes of α-SiC. The evidence indicates though that this is a consequence of rapid growth and not a two-phase "α + β" mixture in the thermodynamic sense. Reflected-light microscopy can be used quantitatively to measure average grain size and shape but cannot resolve most coating defects. Density measurement can be used to differentiate between coatings that exhibit extremes in performance but cannot be used to detect small variations in quality. Scanning electron microscopy shows that deposition variables affect coating surface morphology, but these features are difficult to quantify and do not bear a simple relationship to internal coating defects. Microhardness was a very insensitive indicator of coating quality.

INTRODUCTION

Fuel particles for the High-Temperature Gas-Cooled Reactor (HTGR) consist of uranium-containing microspheres coated with layers of pyrolytic carbon and silicon carbide as shown in Fig. 1. The coatings form a

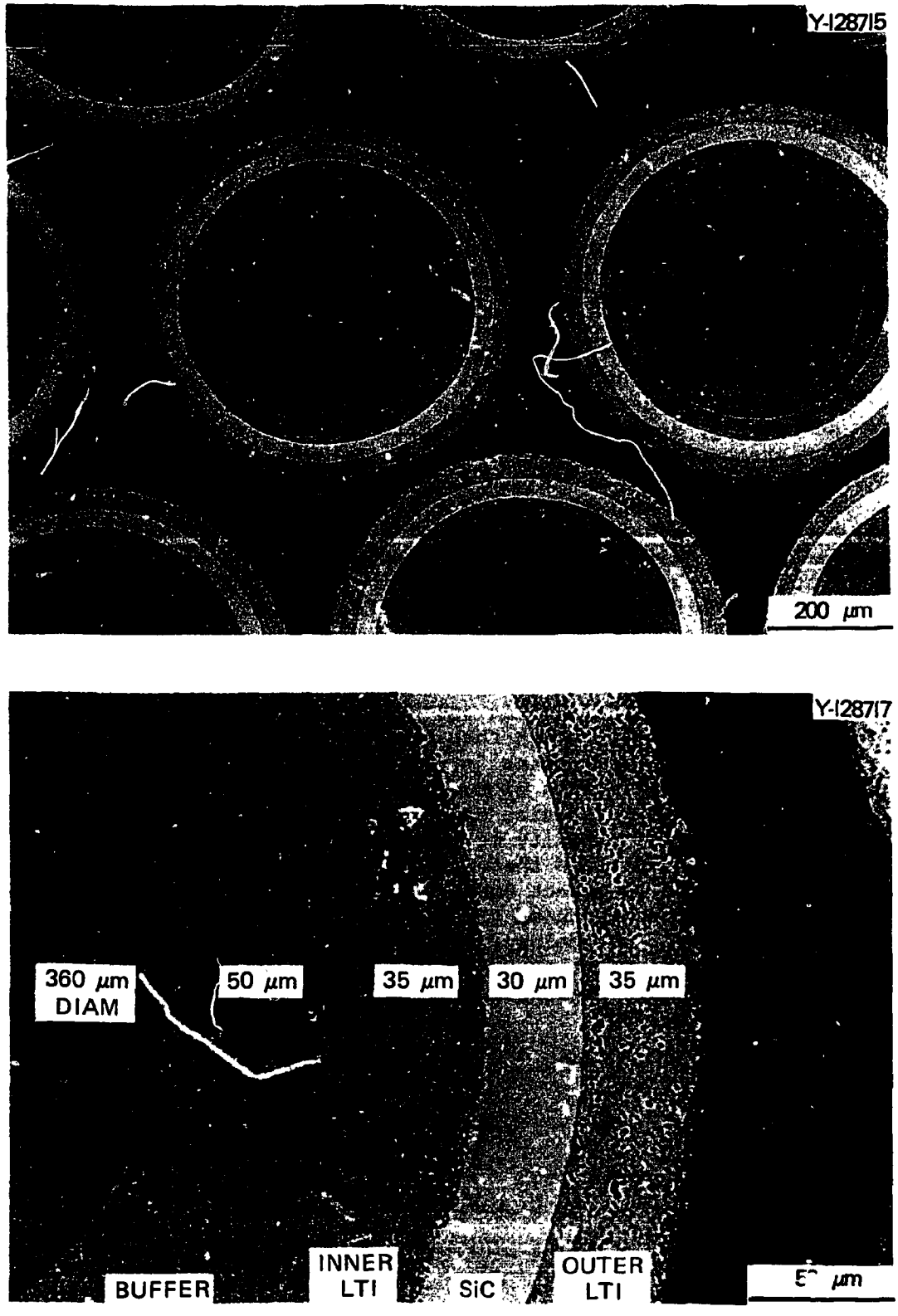

Fig. 1. Coated HTGR Fuel Particles.

miniature pressure vessel around each fuel kernel and serve as the primary containment for fission products. Early work[1] has shown that a dense SiC layer can provide acceptable containment for the fission products formed in high-enriched-uranium (HEU, ~93% ^{235}U) fuels. Recently, interest has developed in the use of low-enriched-uranium (LEU, <10% ^{235}U) fuels. Unfortunately, the fission yield spectra of LEU fuels are different from those of HEU fuels because of the increased ^{239}Pu fissions in the former. A major consequence of the yield spectrum shift is the increased production of noble metals, especially silver and palladium. These elements are particularly aggressive toward SiC at typical fuel operating temperatures in an HTGR.

The primary goal of the SiC development program is to optimize the SiC coating resistance to noble metal transport or attack. To accomplish this it is necessary to characterize the SiC microstructure at the submicron level and then relate microstructural details to both processing variables and performance with respect to noble metal retention. This report evaluates several techniques for characterizing pyrolytic SiC coatings. While each technique has its advantages and disadvantages, the concurrent use of several methods provides the most complete quantitative understanding of SiC microstructures and the affects of deposition variables on them.

SiC COATING PREPARATION AND CHARACTERIZATION METHODS

SiC Deposition

Silicon carbide was deposited on pyrocarbon-coated uranium dioxide microspheres by thermal decomposition of methyltrichlorosilane (CH_3SiCl_3 or MTS) in an excess of hydrogen. Details of the fluidized-bed coating system are given elsewhere.[2] To provide a range of coating types for study and comparision, 12 SiC batches were produced under varied conditions of temperature and coating rate. Deposition parameters for the 12 experimental coating batches are given in Table 1.

Table 1. Experimental Conditions and Results for SiC Deposition

Run	Temperature (°C)	Coating Rate (μm/min)	Density[a] (Mg/m^3)
SC483	1500	0.42	3.208
SC484	1550	0.40	3.212
SC485	1650	0.43	3.218
SC487	1700	0.42	3.197
SC472	1500	0.70	3.190
SC476	1550	0.75	3.207
SC477	1650	0.71	3.203
SC475	1700	0.50	3.195
SC479	1500	1.20	3.156
SC473	1550	1.01	3.195
SC480	1650	0.95	3.207
SC481	1700	1.06	3.206

[a]Standard deviation of coating density measured by the gradient column method is typically ±0.001 to ±0.008 Mg/m^3.

Characterization Techniques

The candidate SiC characterization methods were discussed in detail in a previous report[2] [with the exception of small-angle x-ray scattering (SAXS)]. Application of these techniques to SiC is briefly described below.

Transmission electron microscopy

Coating fragments were removed from the particles and prepared for transmission electron microscopy (TEM) by mixing with aluminum powder and hot-pressing into a pellet according to ORNL Quality Assurance Procedure MET-CER-TS-45. The pellet was diamond sawed, and the resulting slices were mechanically ground and polished before ion milling.[3] After ion milling, the foils were examined in the JEM-100CX electron microscope operating in the following modes: conventional bright-field imaging (diffraction contrast), conventional dark-field imaging, selected-area electron diffraction (SAD), and weak-beam dark-field imaging.

Transmission electron microscopy was used to identify crystallographic phases and determine the type and distribution of defects present.

Small-angle x-ray scattering

The ORNL 10-m SAXS camera and its peripheral computer equipment are described in detail elsewhere.[4] For this work special holders were fabricated to hold the crushed coating samples in the specimen chamber. The holders were made of stainless steel, about 15 by 30 by 0.13 mm thick, with a 7-mm-diam hole in the center. Two thin mylar sheets held the crushed SiC in the hole and served as "windows" through which the x-ray beam could pass without contributing to the scattering. (An empty holder with both windows cemented in place was run along with the 12 containing samples so that background scattering from the windows could be subtracted during data processing.)

The transmission of each specimen was measured by first placing a piece of vitreous carbon in the beam and counting its scattering for 100 s. (The glassy carbon scatters x-rays very strongly over a wide range of angles.) Then the sample was placed into the beam behind the glassy carbon and counted for 100 s. The total integrated intensity with both specimen and carbon was divided by the total intensity without the specimen to obtain the transmission, t (typically $0.3 < t < 0.5$). Then the glassy carbon was removed from the beam, the power was increased, and the scattered intensity from the SiC was counted for 1000 s.

The SAXS camera has a two-dimensional position sensitive detector with a 64 by 64 element array. The data from each run were stored on disk for later processing. At that time the data were recalled, corrected for detector sensitivity and background scattering, and plotted as a two-dimensional map, as shown in Fig. 2. Each contour line represents a doubling in intensity (decreasing from the center outward). After the corrected intensity was displayed as a contour map and shown to be isotropic, a circular average was calculated by the computer. This reduced the data to the form shown in Fig. 3, where scattered intensity is shown as a function of scattering angle. In that form the data are used to determine the defect size range in the material.

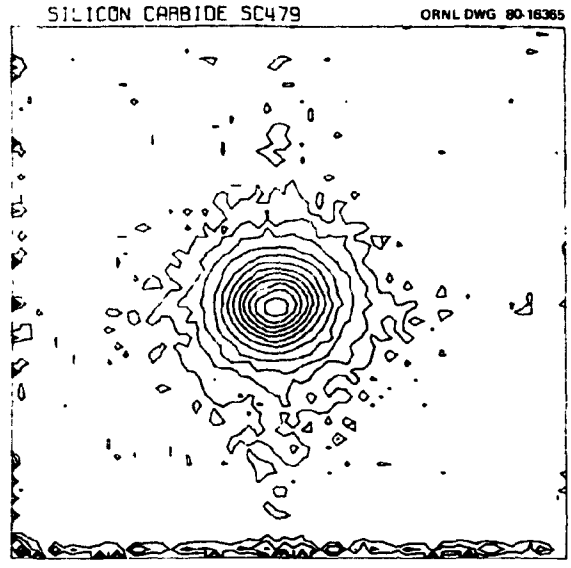

Fig. 2. Scattered X-Ray Intensity from SiC Batch SC479. The lines are isointensity contours, with each contour representing a doubling in intensity level.

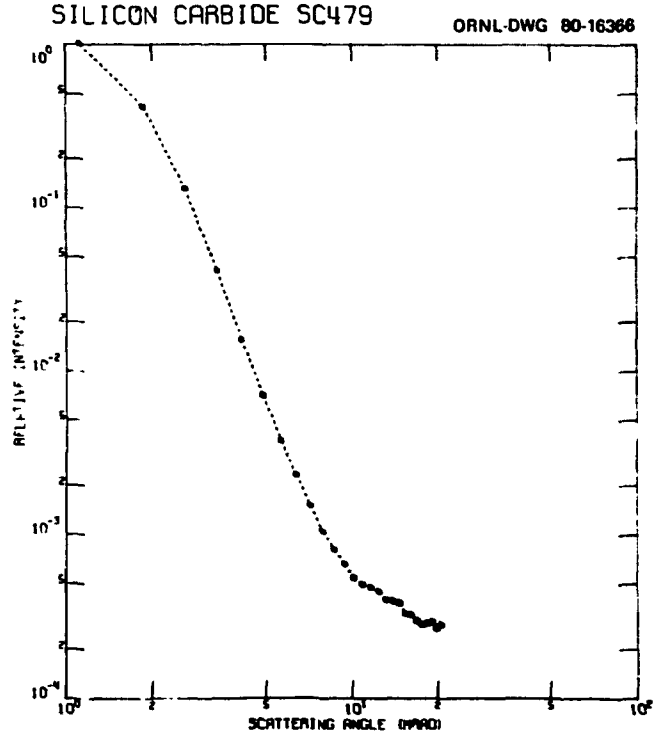

Fig. 3. Small-Angle X-Ray Scattering Curve for SiC Batch SC479. The size range of defects (e.g., voids) present can be calculated from the scattering curve.

X-ray diffraction

Pyrolytic SiC deposited from 1500 to 1700°C has generally been assumed to be pure β-SiC. In this work x-ray diffraction was used to look for traces of α-SiC or other potentially undesirable phases. To keep the background as low as possible, the SiC fragments were mounted on the surface of a specially polished silicon single crystal. As a result, subtle features in the diffraction patterns could be studied.

Optical microscopy

Whole coated particles were mounted in epoxy and ground and polished to midplane according to ORNL Quality Assurance Procedure MET-CER-TS-39. General microstructural features were observed by reflected-light microscopy. Grain sizes were measured in both the radial (growth) and tangential (transverse) directions. Relatively large-scale defects were barely visible at a magnification of 1000.

Density

Coating densities were measured in a liquid density gradient column according to ORNL Quality Assurance Procedure MET-CER-TS-18 by using a mixture of tetrabromoethane and diiodomethane such that the density of the liquid was about 3.15 Mg/m^3 at the top and about 3.22 Mg/m^3 at the bottom of the column. The theoretical density of SiC is about 3.213 Mg/m^3, and current fuel specifications require a minimum SiC density of 3.18 Mg/m^3 (99% of theoretical).

Scanning electron microscopy

Whole particles were examined by scanning electron microscopy (SEM) to study the surface morphology of the SiC layer. The particles were mounted on a brass stub with double adhesive tape and coated with a thin layer of gold to prevent charge buildup. Particle surfaces were photographed at magnifications ranging from 300 to 3000.

Microhardness

Microhardness was measured on each of the 12 coating batches by using a Knoop indentor with a 75-g load. The data were plotted for several orientations (i.e., with the long axis of the indentor radial, tangential, or oblique). In general, there was much scatter in the data. To obtain realistic values, data for all orientations were averaged together for each coating. Average microhardness was then plotted as a function of coating parameters.

RESULTS AND DISCUSSION

Transmission Electron Microscopy

The grain size in SiC coatings, particularly those deposited from 1500 to 1550°C, is about 1 μm. Thus, studying these microstructures optically, beyond measuring average grain sizes, is difficult. Any porosity is well below the resolution limit of optical microscopy. Other crystal defects, such as dislocations, stacking faults, etc. are, of course, even smaller and can be studied conveniently by TEM.

A typical transmission electron micrograph of a thinned coating sample is shown in Fig. 4. The complexity of the microstructure is evident. Numerous dislocations and stacking faults are visible, as well as a cavity where several grain boundaries come together. A previous report[5] showed that TEM results agreed with optical measurements of SiC grain size vs deposition temperature.

The small cavities visible by TEM are believed to be a significant microstructural feature since they probably affect coating strength and performance more strongly than dislocations and stacking faults do. Figure 5 shows a boundary between two SiC grains with three small cavities lying along it. From left to right in the figure the three cavities are approximately (taking the average of major and minor axes) 46, 40 and 110 nm. These numbers are to be compared with SAXS results since they can provide a measure of the size and concentration of voids in the material.

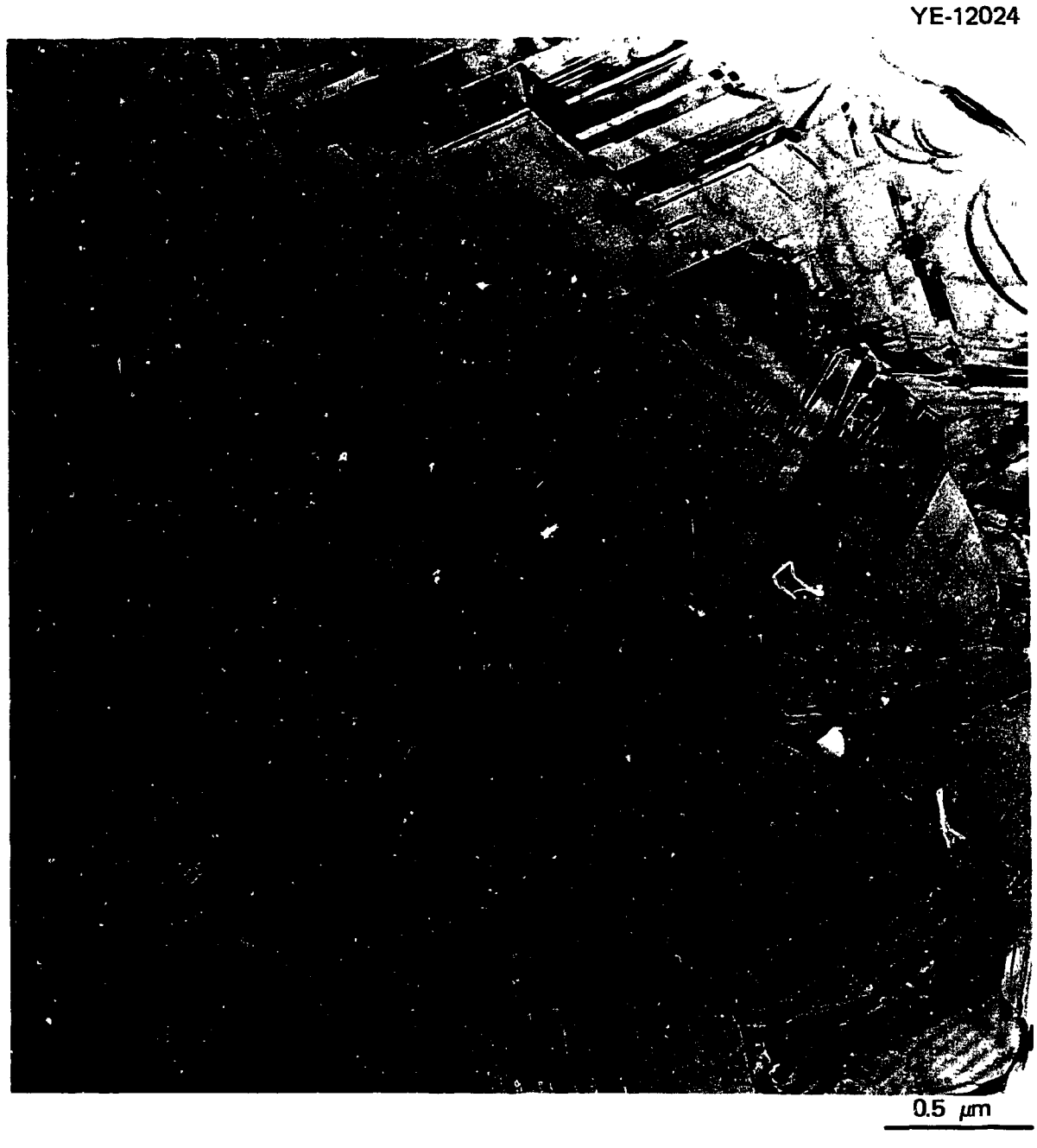

Fig. 4. Transmission Electron Micrograph of Coating SC476 Showing Small Grains, Stacking Faults, Dislocations, and a Polygonal Void.

Fig. 5. High-Magnification Transmission Electron Micrograph of Coating SC476 Showing Small Cavities Along a Grain Boundary.

Micrographs of the following coating batches were surveyed to determine the sizes of cavities present: SC476, deposited at 1550°C at a coating rate of 0.75 μm/min; SC472, deposited at 1500°C at a rate of 0.70 μm/min;

SC483, deposited at 1500°C at a rate of 0.42 μm/min; and SC475, deposited at 1700°C at a rate of 0.50 μm/min. The cavity sizes in nanometers were

SC476	SC472	SC483	SC475
110.0	40.0	40.5	117.5
46.0	17.0	44.0	58.8
40.0	51.5		
82.5	73.5		
46.5	20.0		
66.0	47.5		
88.0	14.5		
44.0	25.5		
70.5	69.5		
106.0	58.5		
59.0	36.5		
29.5	25.5		
47.0	33.0		
	46.5		
	26.5		
	66.5		

Selected-area electron diffraction patterns were used to identify the phases present. The coatings were almost exclusively the 3C (cubic) or β-SiC polytype. However, the high stacking fault density gave rise to streaking in some diffraction patterns (Fig. 6), and occasionally the streaks could be resolved into spots,[2] for which the spacing could possibly be indexed as several noncubic polytypes. Lattice fringe images in one small region had a spacing of 15 nm, which is characteristic of the 6H polytype.[2] It is important to note that stacking faults in SiC are relatively low-energy structures and occur frequently during growth of SiC by chemical vapor deposition. When the stacking faults have a certain sequence in a very localized region of the coating, that region becomes,

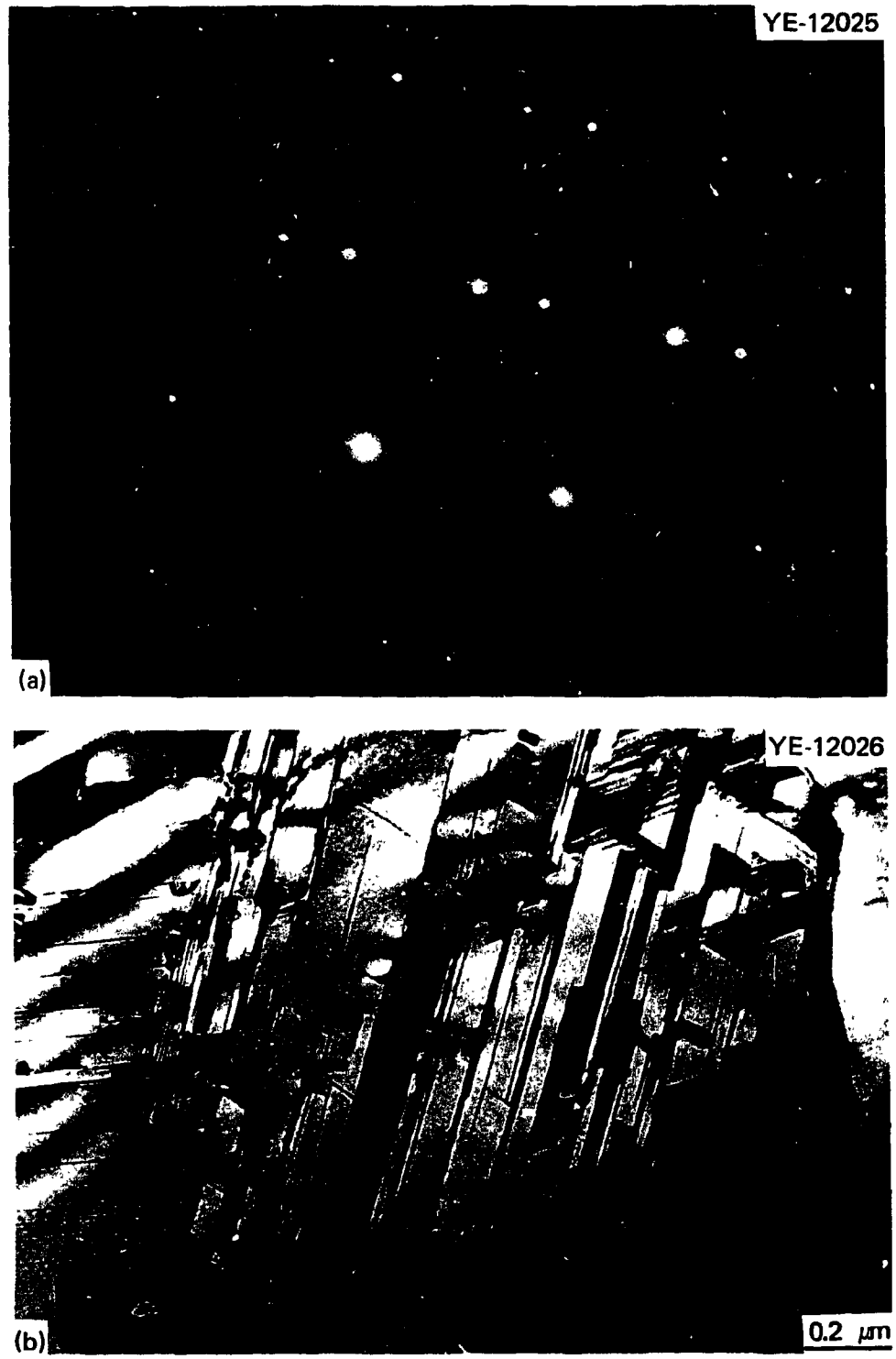

Fig. 6. Transmission Electron Micrograph of Coating SC472, Showing a Heavily Faulted Grain (Below) and the Diffraction Pattern from This Region (Above). The streaks in the diffraction pattern result from the high stacking fault density.

by definition, one of the α-SiC polytypes. But since the coating is not a two-phase mixture in the thermodynamic sense, it is perhaps more accurate to describe the coatings as heavily faulted β-SiC. We believe this designation to be most appropriate since no SiC sample examined in the SAD mode gave a clear diffraction pattern having exclusively the symmetry of an α-SiC polytype. Also, no diffraction spots corresponding to free silicon were detected in any SAD pattern.

The high resolution available in TEM also makes possible the detailed study of changes occurring in SiC coatings during irradiation. Early work[6] reported the irradiation behavior of flat sheets of SiC that had been deposited on graphite disks and carefully stripped off. Unfortunately, the microstructures of coatings deposited on disks are not truly representative of those deposited on microspheres. For the present work, coatings were deposited on carbon microspheres and irradiated in capsule HRB-13 to a fast fluence of about 7×10^{25} neutrons/m^2 (>29 fJ) at 1050°C. These "dummy" particles were broken and the carbon kernels and pyrolytic carbon coating layers were oxidized by heating in air. The SiC coating fragments were mounted as before[3] and studied by TEM.

Figure 7 shows a typical irradiated SiC microstructure. Numerous voids are present, having diameters of about 2.0 to 5.0 nm. Stacking faults have almost disappeared and are much less clearly defined than they were in the as-deposited condition (Fig. 6). Most grain boundaries had a zone on either side that was depleted of voids. This would be expected since grain boundaries are a sink for vacancies and as such would reduce the local vacancy concentration consequently inhibiting void formation.

Small-Angle X-Ray Scattering

Small-angle x-ray scattering is used to study the size distribution and volume concentration of crystal defects or second phases. The SAXS method detects local changes in electron density in the sample material. Silicon carbide, for example has about 95×10^{28} electrons/m^3 while pure

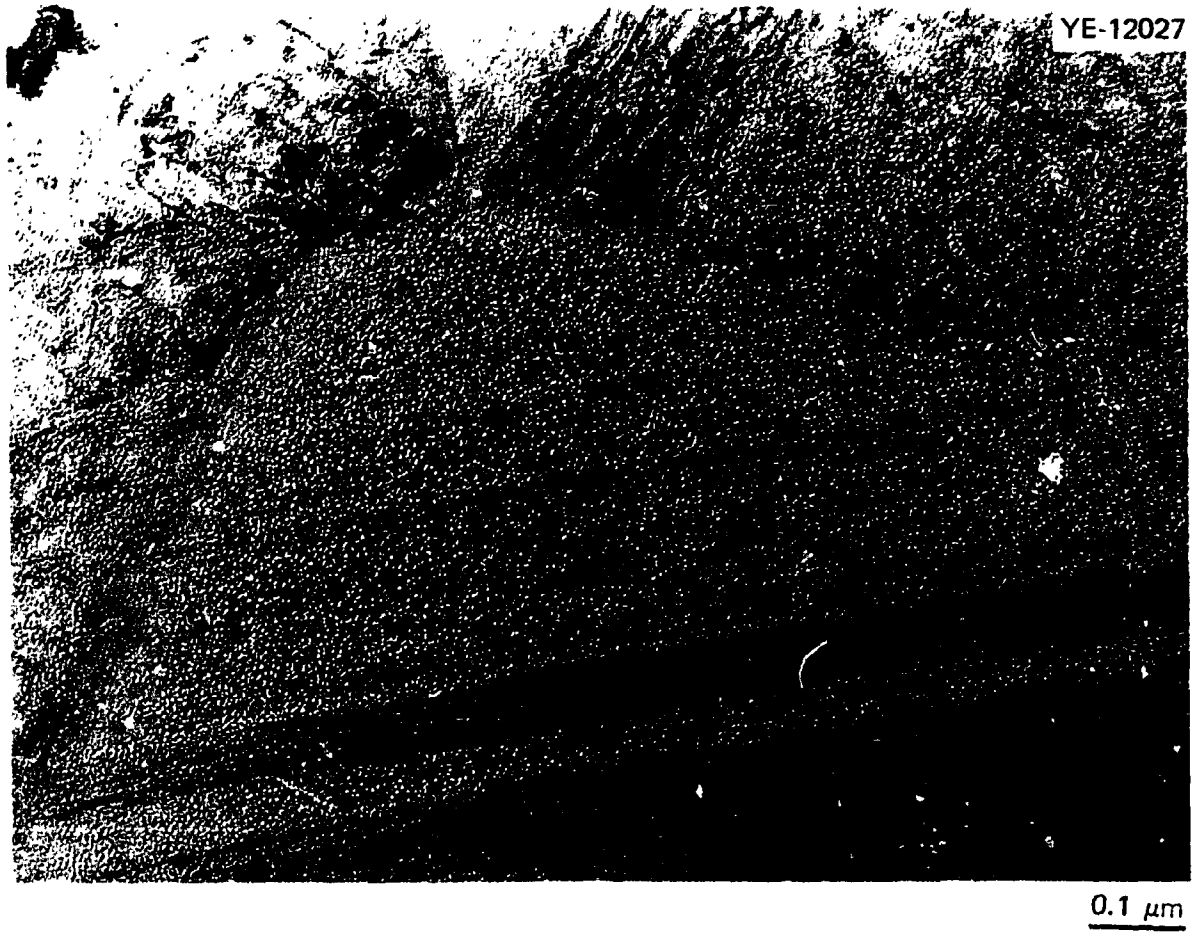

Fig. 7. Silicon Carbide Coating SC272 Irradiated to a Fluence of About 7×10^{25} neutrons/m^2 (>29 fJ). Note small voids, depleted zones around grain boundaries, and remnants of stacking faults.

silicon has about 70×10^{28} electrons/m^3. This difference is theoretically detectable if enough free silicon were present. Voids, of course, have essentially no electrons and thus are easily detected. Stacking faults, dislocations, and grain boundaries are not detected since they do not represent a significant change in the electron density. It is important to note that SAXS does not provide information on the nature of the defects but only on their size distribution. Thus, SAXS can be used in conjunction with TEM to better understand the size and type of defects present.

Scattering curves were obtained for each of the 12 SiC batches. The data were analyzed by the Guinier method according to the following relation:

$$I_s = I_0 \exp(-R_g^2 \kappa^2/3) \ , \tag{1}$$

where

I_s = scattered intensity at a particular angle,
I_0 = scattered intensity at $\theta = 0$,
R_g^2 = mean square radius of gyration of scattering objects,
$\kappa = (4\pi/\lambda) \sin(\theta/2)$,
λ = x-ray wavelength.

A plot is made of $\log I_s(\theta)$ vs θ^2, and the slope, S, of the plot is given by

$$S = [\log I(\theta_1) - \log I(\theta_2)] / \left(\theta_1^2 - \theta_2^2\right) . \tag{2}$$

The mean radius of gyration, R_g, is then

$$R_g = 0.645 \sqrt{-S} \ . \tag{3}$$

If the scattering objects are approximately spherical, then

$$R = \sqrt{5/3} \, R_g \ , \tag{4}$$

where R = radius of spherical defects.

If the scattering objects (defects) have a narrow size range, the "Guinier plot" of $\log I$ vs θ^2 will form a straight line. If the plot has two straight segments forming an "elbow," it indicates that the defects have a biomodal size distribution. A typical Guinier plot for our data has

pronounced curvature, as shown by Fig. 8. This implies either a multimodal or a continuous distribution of defect sizes. The size range of the defects in each sample can be estimated by approximating the two ends of the curve by straight line segments. From the two slopes shown in Fig. 8, $R_{max} \approx 38.0$ nm and $R_{min} \approx 11.0$ nm. This implies that the majority of the defects lie in the range 22.0 to 76.0 nm in diameter. These values are in reasonable agreement with those presented on p. 11 when one recalls that the voids are rarely spherical. They are at best polygonal and sometimes lens- or dumbbell-shaped. Another point to remember is that TEM cannot achieve the comprehensive sampling that SAXS does.

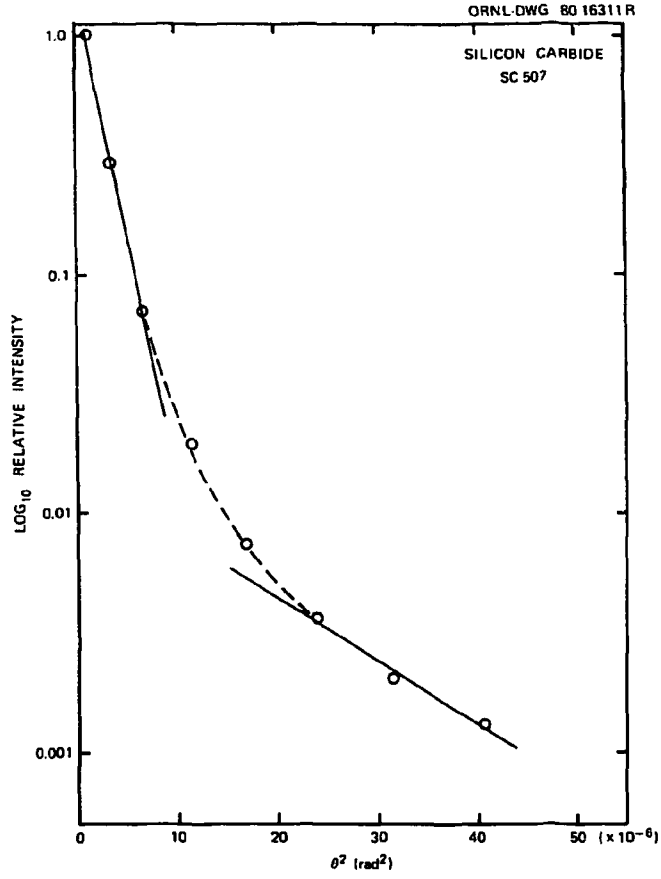

Fig. 8. Guinier Plot of Small-Angle X-Ray Scattering Curve for Coating SC507. The two slopes indicate that the defects (voids) mostly range from 22.0 to 76.0 nm in diameter.

All coatings examined by SAXS had very similar values for R_{max} and R_{min}, and defect size vs coating conditions had no discernable trend. To compare one coating batch with another, therefore, the total integrated intensities (corrected for specimen attenuation) are plotted in Fig. 9. The figure shows that the total intensity varies from batch to batch by up to a factor of 2. This implies a similar variation in void concentrations.

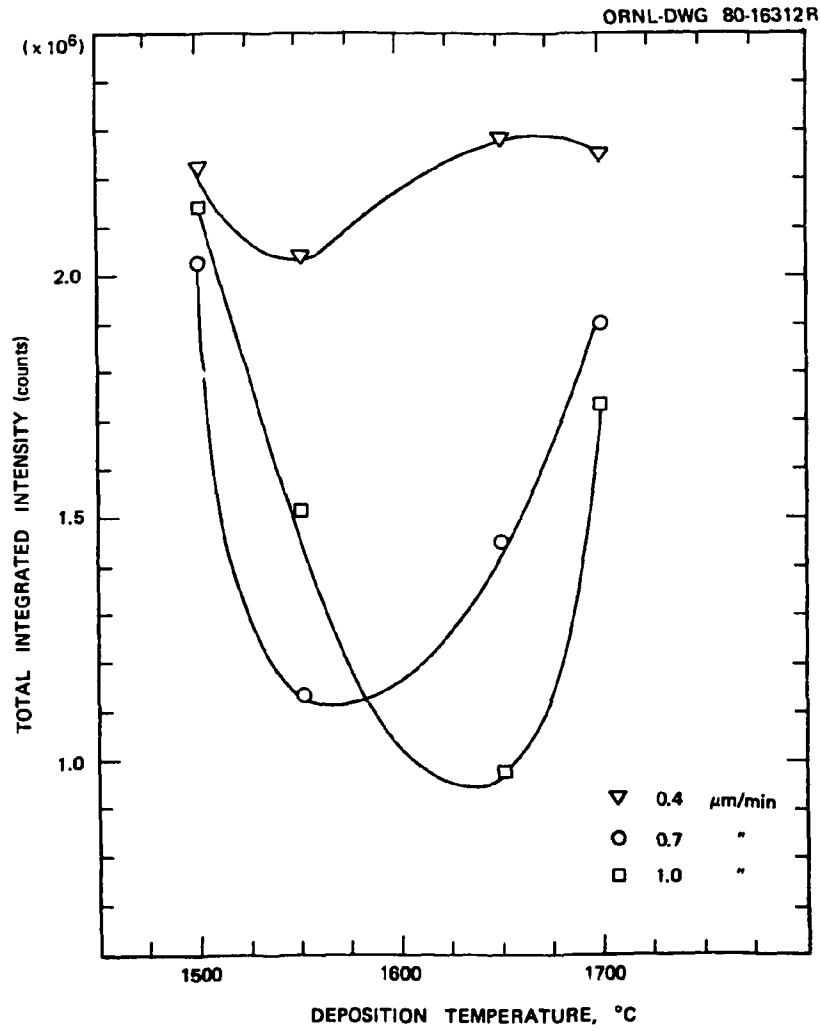

Fig. 9. Total Integrated Small-Angle X-Ray Scattering Intensity for the 12 SiC Batches. The total intensity (and hence void concentration) varies by as much as a factor of 2 when coating parameters are changed.

Another possible way to compare batches is by comparing scattered intensity at one particular angle.[7] Figure 10 shows, however, that data taken at a single scattering angle must be interpreted with care. Taking the three batches deposited at 1500°C as an example, a coating that appears to have fewer defects than another at one angle might appear to have more defects at another angle. Clearly, the entire scattering curve must be examined to adequately characterize the distribution of defects.

X-Ray Diffraction

The 12 experimental SiC batches were analyzed by x-ray diffraction (XRD) along with 4 batches from the 0.13-m coater, 1 sample from earlier work, and 3 batches that were not examined by other techniques. The XRD patterns fell into three categories:

1. strong β-SiC peaks only,
2. strong β-SiC peaks with a weak intensity plateau around 34 to 35°,
3. strong β-SiC peaks with a weak intensity plateau and a few small α-SiC peaks.

Figure 11 illustrates these three XRD pattern types schematically. When the diffraction patterns are related to the coating deposition variables (Fig. 12), it becomes apparent that very high coating rates and/or low temperatures favor traces of α-SiC, while low coating rates and high temperatures favor β-SiC. Between the two extremes lie those conditions that produce the broad, low-intensity diffraction plateau characteristic of a heavily faulted material. This diffraction effect is seen as streaking in electron diffraction [Fig. 6(a)] where the faults are nearly parallel to the electron beam. This observation reinforces the belief that high coating rates favor a high stacking fault density, which in turn increases the chance that small regions can have structures identifiable as particular noncubic polytypes of SiC. The actual mechanism by which these small regions approach the hexagonal structure is probably associated with growth of the coating, and none of these coatings is a two-phase mixture in the thermodynamic sense.

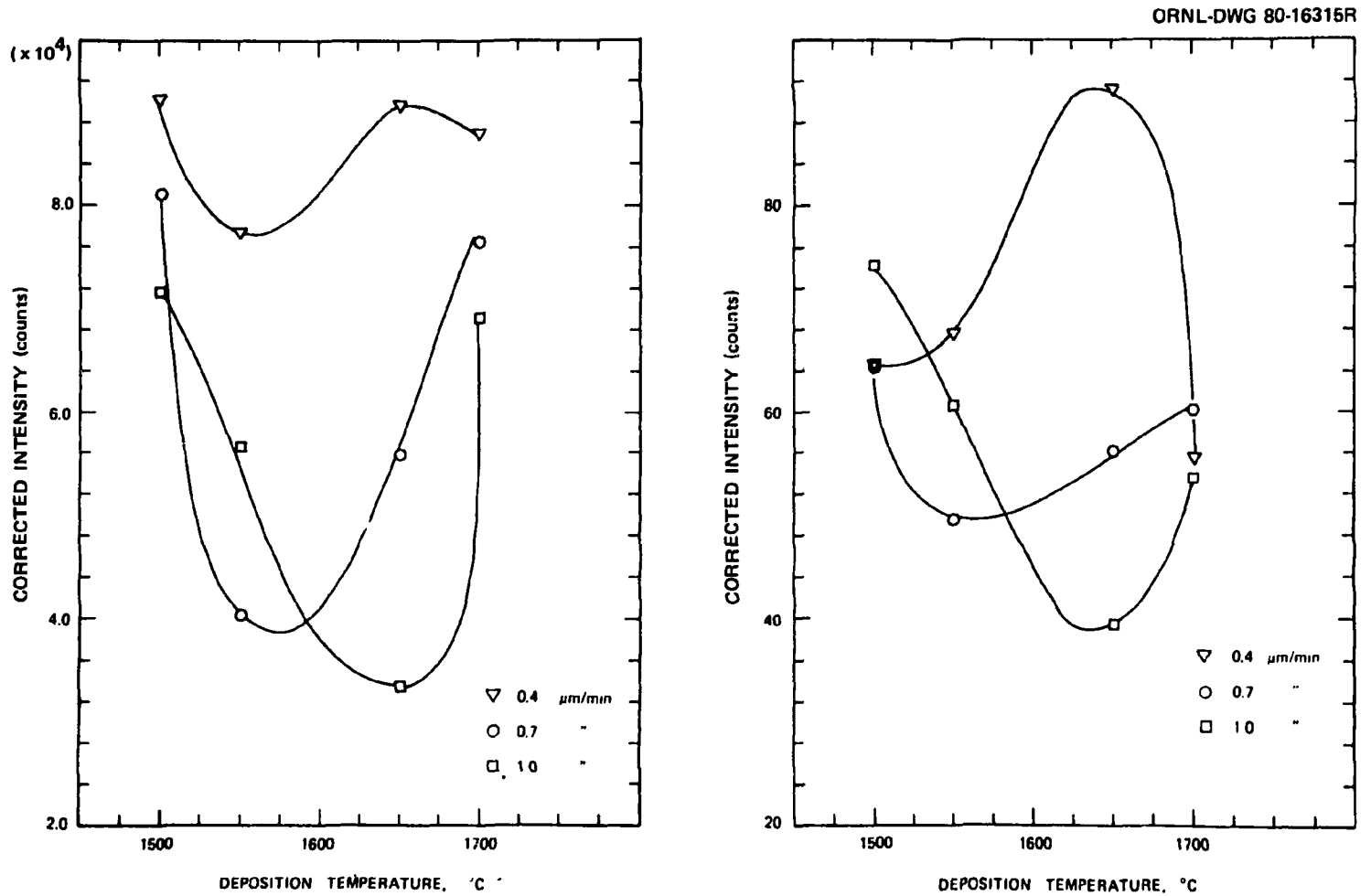

1.12 mrad SCATTERING ANGLE 7.86 mrad

Fig. 10. Comparison of the 12 Coatings by Using X-Ray Scattering at a Single Angle Must Be Interpreted with Care. Apparent relative quality depends strongly on the scattering angle chosen.

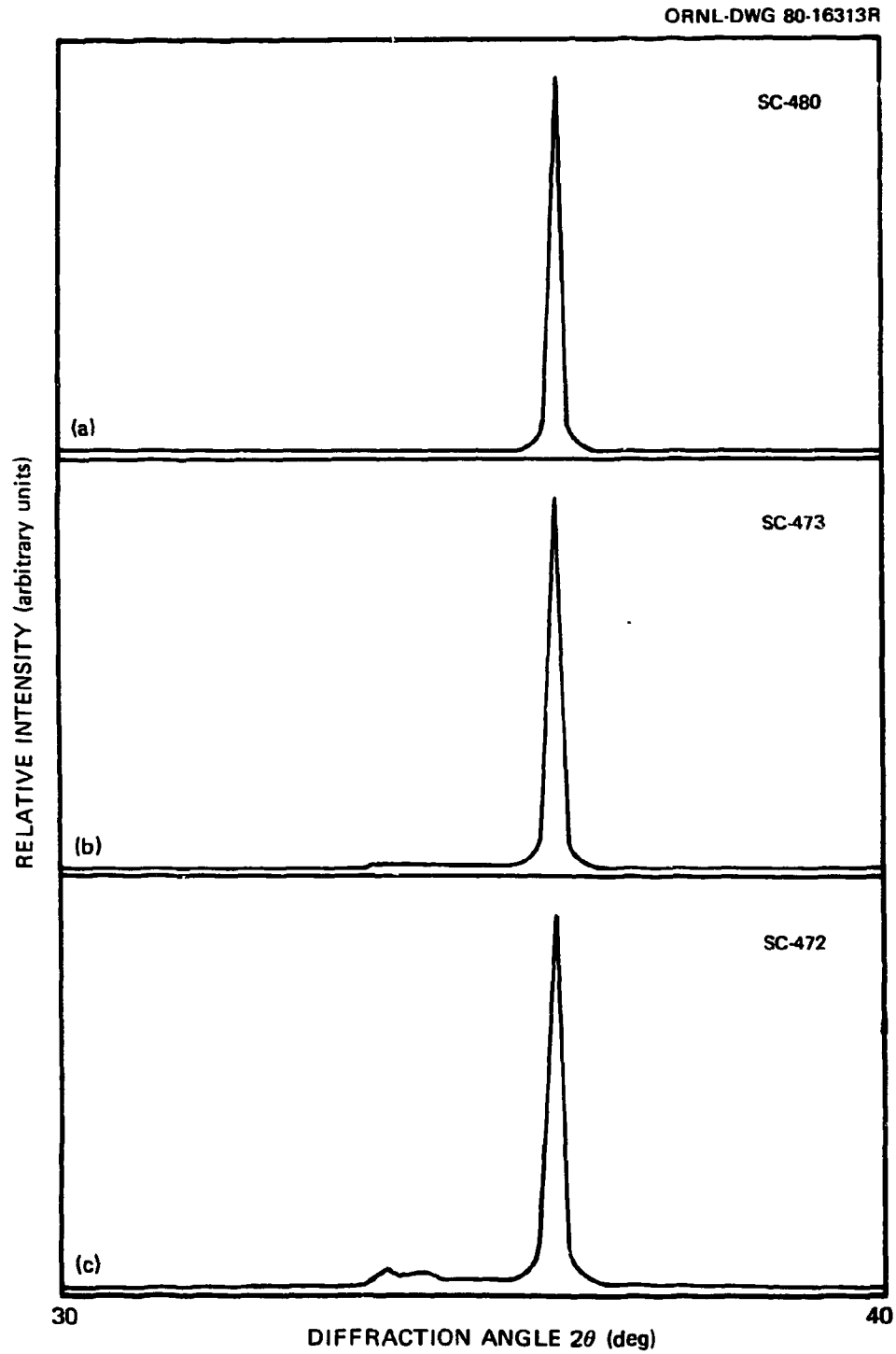

Fig. 11. Schematic X-Ray Diffraction Patterns for SiC Coatings. (a) Pure β-SiC. (b) Pure β-SiC with diffuse plateau, presumably resulting from high stacking fault density. (c) Mostly β-SiC with a trace of "α-SiC."

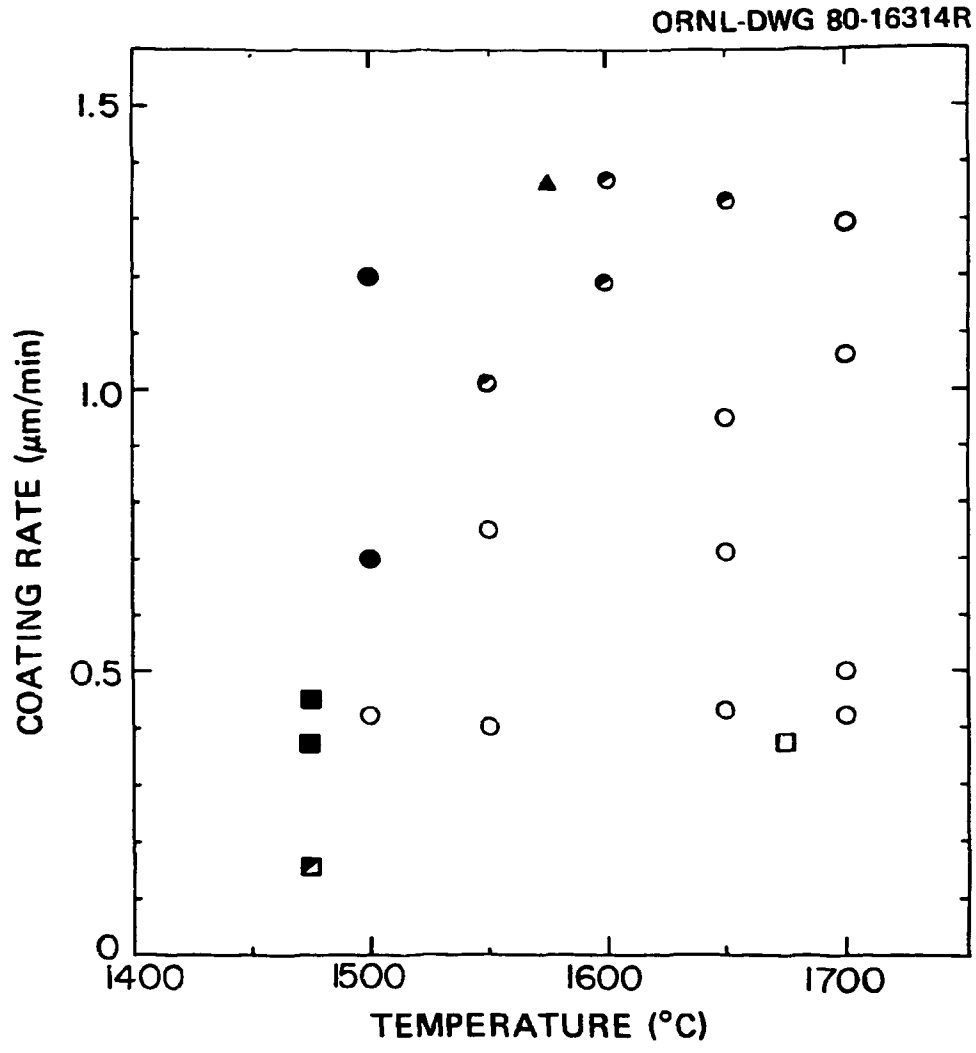

Fig. 12. X-Ray Diffraction Results Are Strongly Related to SiC Deposition Parameters.

Optical Microscopy

While most microstructural features in the coatings are too small to resolve optically, the measurement of average grain size is relatively simple. The grain size could be a key parameter with respect to fission product transport, which might involve grain boundaries. Figure 13 shows that grain size as well as shape (equiaxed or columnar) depend strongly on temperature and coating rate.

The only defects visible optically are dark circumferential striations often seen in coatings deposited at 1500 to 1550°C. The fine structure of this defect was not known until recent transmission electron micrographs identified the striations as bands of very small equiaxed grains with a locally high concentration of intergranular porosity.[5]

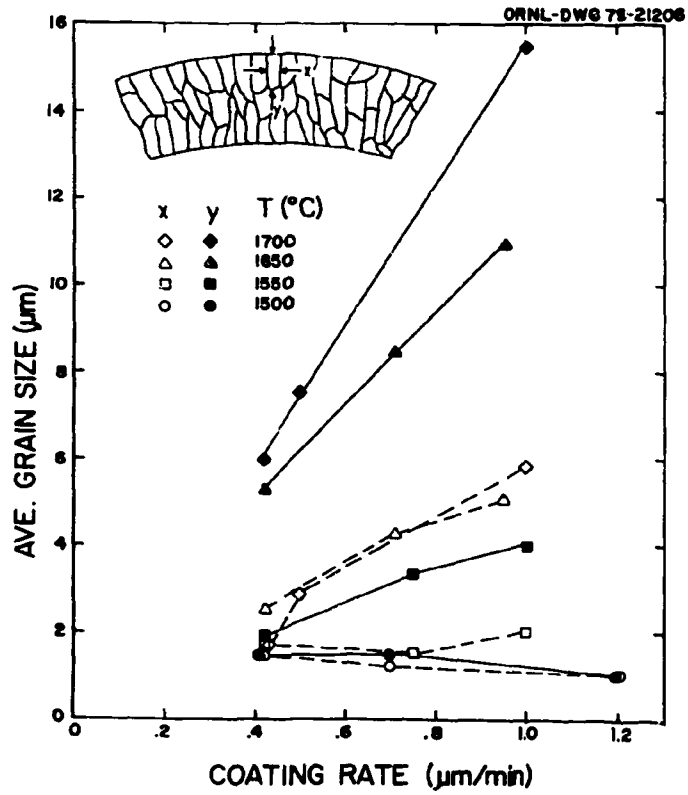

Fig. 13. Silicon Carbide Grain Size and Shape as a Function of Coating Parameters.

Density

In any material where porosity is a major identifiable defect and strength and impermeability are major service requirements, it is logical that density should be an important measure of quality. Coating density is readily measured by immersion in a liquid density gradient column, and current fuel specifications require the SiC to be at least 99% of theoretical density ($\rho_{min} > 3.18$ Mg/m^3).

Density measurement can distinguish unquestionably between very good coatings (near theoretical density) and very bad ones. But when a series of "good" coatings is fabricated under varying conditions, density is not a sensitive measure of their relative quality. Figure 14 shows the densities of SiC batches fabricated for irradiation capsule HT-35 as a function of coating rate. All coatings are well above the specified minimum density. There is virtually no correlation between density and coating rate, and the uncertainty in many of the values is greater than the differences between them.

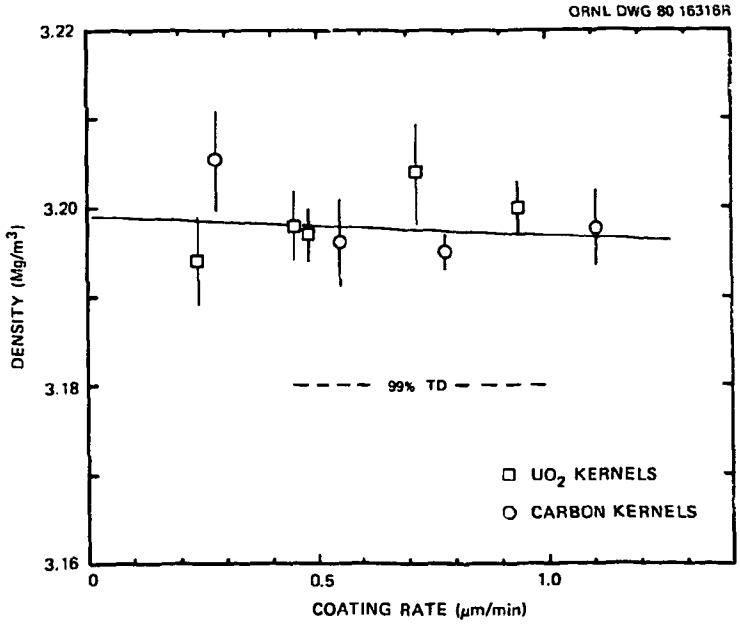

Fig. 14. Densities of SiC Batches for Capsule HT-35. The data show no clear correlation between density and coating rate.

Scanning Electron Microscopy

Previous reports[2,5] have shown that the surface morphology of SiC, as revealed by SEM, is strongly dependent on deposition parameters. Low-temperature coatings have a botryoidal or globular surface, while very high-temperature coatings often exhibit gaps between the grains on the surface. Coating rate also influenced surface morphology. In general, highly dense coatings had surfaces of blocky, interlocking grains with well-developed faces and no obvious gaps in between. Less dense coatings had various other surface features.

Use of SEM as a characterization technique has several major drawbacks. First, it is impossible to analyze scanning electron micrographs as objectively and quantitatively as optical micrographs. Second, it is difficult to tell the depth of surface defects. The grain boundary gaps seen in some high-temperature deposits certainly do not go all the way through the coating thickness. Third, the outer surface is probably the least important part of the SiC layer. (Perhaps more useful information might be gained by examining the *inner* surface of the SiC.)

Microhardness

Metallographically prepared coated particles were tested to determine if microhardness is a sensitive indicator of coating quality. The Knoop microhardness number (KHN)[8] for pure SiC is 2480. Values for the SiC coatings tested were generally in this vicinity, but the scatter in the data is significant. The coatings deposited at the lowest coating rate had the widest variation in hardness within a given coating batch. Some of these coatings happened to be thinner than desired, and this is believed to be the main source of error.

Microhardness of coatings deposited at 0.7 μm/min reaches a maximum at a deposition temperature of about 1600°C and decreases rapidly above 1650°C as shown in Fig. 15. The uncertainty in the data is still appreciable, but not as severe as in those coatings deposited at lower

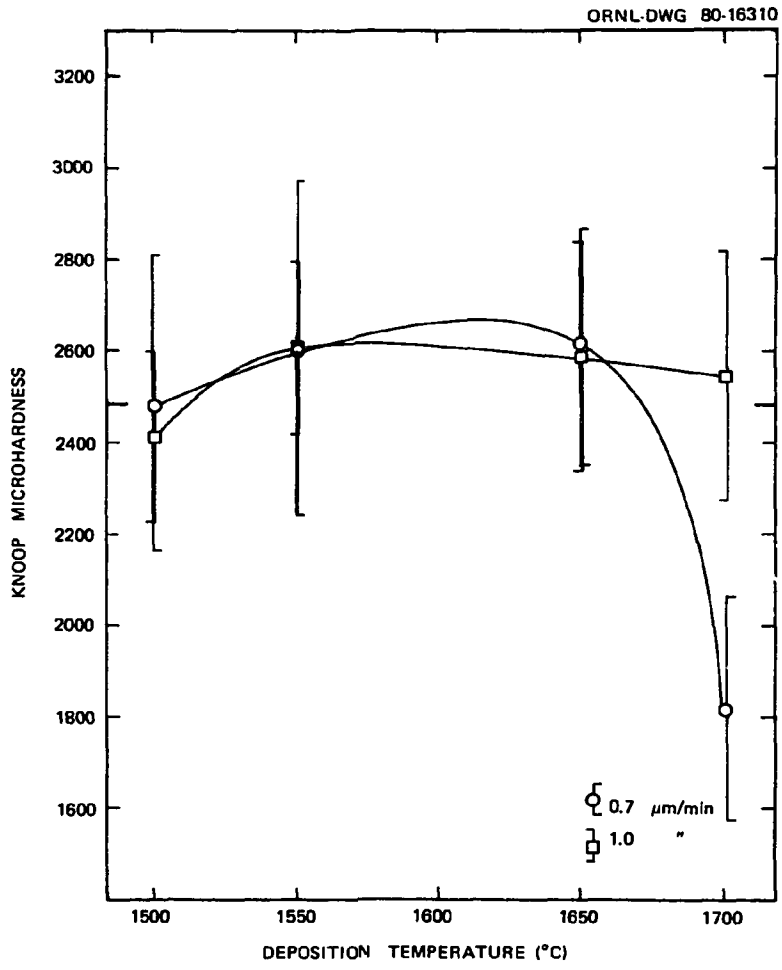

Fig. 15. Knoop Microhardness of SiC Coatings vs Deposition Temperature for Two Different Coating Rates.

coating rates. Coatings deposited at 1.0 μm/min show appoximately the same behavior as those deposited at 0.7 μm/min, but the data scatter has narrowed somewhat. Some of these coatings were slightly thicker than usual, and the added thickness could have helped prevent cracking during hardness testing. The hardness data for coatings deposited at 0.7 and 1.0 μm/min suggest that microhardness is not a sensitive measure of coating quality. Batch-to-batch variations in hardness are smaller than particle-to-particle variations. In qualitative terms, it is not surprising that microhardness appears to reach a maximum in the same temperature range where density reaches a maximum.

CONCLUSIONS

1. Details of the grain structure of SiC coatings and the defects in them were observed by TEM. Major crystal defects included voids, stacking faults, and dislocations. Free silicon was not found in any of the SiC batches examined.

2. Small-angle x-ray scattering is a powerful tool for characterizing the size distribution of coating defects. It has the statistical advantage of sampling a larger volume of material than TEM does. The disadvantage of SAXS is that taken alone it does not identify the nature of the defects present.

3. The approximate size range of defects in the coatings examined by SAXS is about 20.0 to 80.0 nm in diameter and is independent of coating parameters in the range studied here. Transmission electron microscopy identified the defects as voids and gave qualitative agreement on their sizes.

4. X-ray diffraction indicates that coatings deposited at relatively low temperatures and/or high coating rates have a high density of stacking faults. In some very small areas the heavily faulted structure resembles one or more polytypes of α-SiC. However, the evidence indicates that this is a consequence of rapid growth and not a two-phase "$\alpha + \beta$" mixture in the thermodynamic sense.

5. Reflected-light microscopy can be used to quantitatively measure grain size and shape. Trends of grain size vs deposition parameters have been confirmed by TEM. Most coating defects, however, are well below the resolution capability of optical microscopy.

6. The immersion technique can be used to identify very dense SiC coatings. However, it cannot be used to determine which of several high-density SiC variants will perform best during irradiation.

7. Scanning electron microscopy shows that deposition variables definitely affect coating surface morphology. However, the surface features visible in scanning electron micrographs are difficult to quantify and do not bear a simple relationship to internal coating defects.

8. Microhardness is not a sensitive indicator of SiC coating quality. The problems involved with measuring the microhardness of a brittle material are compounded by the small size of the coating in cross section and make accurate, reproducible measurements nearly impossible.

9. The SiC microstructures can be characterized most completely by using quantitative TEM and SAXS together.

ACKNOWLEDGMENTS

The authors would like to thank the following persons for their contributions to this work: J. W. Geer prepared the coatings and separated the samples, W. R. Johnson hot-pressed sample fragments in aluminum, H. Keating prepared TEM specimens and measured densities, and W. H. Smith performed the x-ray diffraction measurements. W. H. Warwick prepared metallographic specimens and S. S. Rawlston measured microhardness.

J. S. Lin, G. D. Wignall, and R. W. Hendricks assisted with SAXS, and T. J. Henson performed SEM.

T. N. Tiegs and M. J. Kania reviewed the manuscript. The final draft was edited by B. G. Ashdown and K. A. Witherspoon prepared and assembled the final report for publication.

REFERENCES

1. T. D. Gulden and H. Nickel, "Preface, Coated Particle Fuels," *Nucl. Technol.* 35: 206–13 (September 1977).
2. R. J. Lauf, D. N. Braski, and V. J. Tennery, *Characterization of SiC Coatings on HTGR Fuel Particles: Preliminary Report*, ORNL/TM-6940 (August 1979).
3. R. J. Lauf and H. Keating, "Prepartion of Ceramic Particulates for Transmission Electron Microscopy," pp. 196–97 in *38th Annu. Proc. Electron Microscopy Soc. Amer.*, ed. by G. W. Bailey, Claitor's Publishing Division, Baton Rouge, La., 1980.

4. R. W. Hendricks, "The ORNL 10-Meter Small-Angle X-Ray Scattering Camera," *J. Appl. Crystallogr.* 11: 15–30 (1978).

5. R. J. Lauf and D. N. Braski, *Dependence of Silicon Carbide Coating Properties on Deposition Parameters: Preliminary Report,* ORNL/TM-7209 (May 1980).

6. R. J. Price, "Effects of Fast-Neutron Irradiation on Pyrolytic Silicon Carbide," *J. Nucl. Mater.* 33: 17–22 (1969).

7. P. Krautwasser and E. Wallura, "Silicon Carbide Characterization by Small-Angle X-Ray Scattering," paper presented at ANS Winter Meeting, San Francisco, Nov. 11–15, 1979.

8. L. S. Foster, "Comparison of Hardness Values of Various Materials on Mohs and Knoop Scales," p. F-24 in *Handbook of Chemistry and Physics,* 60th ed., Chemical Rubber Publishing Co., Cleveland, Ohio, 1979.

ORNL/TM-7571
Distribution
Category UC-77

INTERNAL DISTRIBUTION

1–2. Central Research Library
3. Document Reference Section
4–5. Laboratory Records Department
6. Laboratory Records, ORNL RC
7. ORNL Patent Section
8. P. Angelini
9. R. L. Beatty
10. P. F. Becher
11. J. Bentley
12–16. D. N. Braski
17. A. J. Caputo
18. G. L. Copeland
19. R. G. Donnelly
20. J. I. Federer
21. C. B. Finch
22–24. M. R. Hill
25. F. J. Homan
26. M. J. Kania
27–36. P. R. Kasten
37. W. J. Lackey
38–52. R. J. Lauf
53. B. C. Leslie
54. T. B. Lindemer
55. Jar-Shyong Lin
56. K. H. Lin
57. E. L. Long, Jr.
58. P. J. Maziasz
59. R. E. Norman
60. R. J. Pearson
61. P. L. Rittenhouse
62. P. S. Sklad
63. C. J. Sparks, Jr.
64. J. O. Stiegler
65. D. P. Stinton
66. V. J. Tennery
67. T. N. Tiegs
68. M. J. Mayfield (Consultant)
69. A. L. Bement, Jr. (Consultant)
70. E. H. Kottcamp, Jr. (Consultant)
71. Alan Lawley (Consultant)
72. T. B. Massalski (Consultant)
73. R. H. Redwine (Consultant)
74. John Stringer (Consultant)

EXTERNAL DISTRIBUTION

75–76. DOE, GAS-COOLED REACTOR PROGRAMS DIVISION, Washington, DC 20545

G. A. Newby
J. E. Fox

77. DOE, OFFICE OF ADVANCED NUCLEAR SYSTEMS AND PROJECTS, Washington, DC 20545

Director

78. SAN-DEVELOPMENT, SAN DIEGO AREA OFFICE, P.O. Box 81325, San Diego, CA 92138

Senior Program Coordinator

79. DOE, SAN FRANCISCO OPERATIONS OFFICE — SAN DIEGO, 110 West A Street, Suite 460, San Diego, CA 92101

Manager

80–81. DOE, OAK RIDGE OPERATIONS OFFICE, P.O. Box E, Oak Ridge, TN 37830

Office of Assistant Manager for Research and Development
Director, Nuclear Research and Development

82–246. DOE, TECHNICAL INFORMATION CENTER, P.O. Box 62, Oak Ridge, TN 37830

For distribution as shown in TID-4500 Distribution Category, UC-77 (Gas-Cooled Technology)

☆U.S. GOVERNMENT PRINTING OFFICE: 1980-640-245/432